LaFeO3 thin films as relevant models for the surface investigation of 3-way catalysts

Shreya Nandi, Dimitri Blanck, Thomas Carlier, Marie-Hélène Chambrier, Anne-Sophie Mamede, Martine Trentesaux, Pardis Simon, Nicolas Nuns, Pascal Roussel, Anthony Ferri, et al.

$LaFeO_3$ thin films as relevant models for the surface investigation of three-way catalysts

Shreya Nandi[†], Dimitri Blanck[†], Thomas Carlier[‡], Marie-Hélène Chambrier[‡], Anne-Sophie Mamede[†], Martine Trentesaux[†], Pardis Simon[†], Nicolas Nuns[§], Pascal Roussel[†], Anthony Ferri[‡], Jean-François Paul[†] and Elise Berrier[†,⋆]

†*Univ. Lille, CNRS, ENSCL, Centrale Lille, Univ. Artois, UMR 8181,UCCS - Unité de Catalyse et Chimie du Solide, F-59000 Lille, France*

‡*Univ. Artois, CNRS, Centrale Lille, ENSCL, Univ. Lille, UMR 8181, Unité de Catalyse et Chimie du Solide (UCCS), F-62300 Lens, France*

§*IMMCL Chevreul, Institut des Molécules et de la Matière Condensée, F-59650 Villeneuve d'Ascq, France*

⋆ Corresponding author: Elise.Berrier@univ-lille.fr

Note: This is the peer reviewed version of the following article: Nandi, S., Blanck, D., Carlier, T., Chambrier, M. H., Mamede, A. S., Trentesaux, M., Simon, P., Nuns, N., Roussel, P., Ferri A., Paul, J. F. and Berrier E. (2018). $LaFeO_{3\pm\delta}$ thin films as relevant models for the surface investigation of 3-way catalysts. Surface and Interface Analysis, 50(11), 1018-1024., which has been published in final form at https://doi.org/10.1002/sia.6450. This article may be used for non-commercial purposes in accordance with Wiley Terms and Conditions for Use of Self-Archived Versions.

Abstract: Lanthanum orthoferrite, a highly potential three-way catalyst, shaped as apolycrystalline thin film has been comprehensively analysed by combining bulk and surface characterization techniques. The possibility to accomplish unprecedented surface information has been presented, thanks to the combined use of LEIS, XPS and ToF-SIMS. The structural, morphological and surface properties at nano-metric scale make such thin films indistinguishable from powdered solids. Thus, the relevance of using such model materials for advanced surface investigations of $LaFeO_{3\pm\delta}$-based three-way catalysts has been demonstrated.

Keywords: perovskite, $LaFeO_3$, Raman, XPS, ToF-SIMS, LEIS

1 Introduction

$LaFeO_{3\pm\delta}$ (LFO) solids showing ABO_3 perovskite structure have been demonstrated to be smart support materials in three-way catalysis (TWC) for the simultaneous abatement of CO, NO and unburnt hydrocarbons in the catalytic converters of automotive engines. Their application in such a system is highly suitable owing to their structural thermal stability under redox conditions [1], the possibility to fine-tune their composition by substitution in A and/or B site(s) [2] and their consistent oxygen storage capacity (OSC) [3].

In heterogeneous catalysis, only the outermost atomic layers of the active material, being in contact with the reactants, can directly participate in the reaction. On the other hand, the subsurface can help in maintaining and/or regenerating the active phase, which is the starting point of the key concept of *self-regeneration* [4, 5]. Moreover, it was recently shown that the composition of the perovskite oxide plays a key role in the regeneration process. In return, the versatile composition of oxide perovskite materials can help improving this crucial benefit [6]. In the context of reducing the amount of critical raw materials while maintaining a high activity in TWC, lanthanum perovskite materials with extremely low to zero noble metal content nowadays appear as quite a promising entry to the formulation of future 3-way catalysts [7]. Quite recently, we have reported on an *in situ* Raman study of $LaFeO_{3\pm\delta}$ and proposed that the surface composition and reconstruction played a crucial role in TWC performances [8]. More precisely, the mobility of FeO_6 moieties in and out the LFO lattice upon redox cycling was proposed to take part in the activity enhancement of La-deficient materials [9]. Following this hypothesis lies the capacity of iron-based moieties to move reversibly from the sub-surface to the surface mediated by the precipitation of small Fe_2O_3 nanoparticles.

Shaping $LaFeO_{3\pm\delta}$ as Si-supported, polycrystalline thin films is expected to yield few layers of nanocrystallites and hence, provide a chance for a better description of the active phase located on the catalyst's (sub)surface. In practice, such thin films are also likely to favour a more suitable surface analysis. For example, perovskites shaped as thin films make it possible to afford an elemental depth profiling using ToF-SIMS, which is not as efficient with the corresponding powders. Distantly adapted from the well-accepted concept of investigating monocrystalline surfaces as model active materials [10], the flat model catalyst approach we apply here, however, does not involve such a material gap [11, 12]. To the best of our knowledge, the application of this method is original in the investigation of catalytically relevant $LaFeO_3$ thin films. Such a model material paves the way to a clear depiction of the surface and sub-surface that determine the catalytic behaviour of active bulk materials. However, an obvious prerequisite to the use of $LaFeO_{3\pm\delta}$ thin films as convenient model shapes for in-depth surface analyses lies in the structural and textural analogy with lab-scale active materials, such as powdered catalysts. The present work aims at clarifying the relevance of polycrystalline thin films in being used as a model surface/sub-surface system for investigating $LaFeO_{3\pm\delta}$-based three-way catalysts.

2 Materials and Methods

2.1 Preparation of polycrystalline LFO thin films

The preparation of the precursor sol was largely based on the one of Liu *et al.* for preparing alumina supported $LaFeO_{3\pm\delta}$ films[13]. 0.65g of lanthanum nitrate hexahydrate (99.9 %, Aldrich) and 0.61 g of iron nitrate nonahydrate (99.9 %, Aldrich) were diluted in millipore water (15.0 MΩcm at 17 °C) for preparing 5 mL of bimetallic solution having a metal concentration of [Fe]=[La]=0.3 mol L^{-1}. The solution was transferred in a round flask and vigorously stirred. Citric acid (99.5 %, Sigma-Aldrich) was

then added in order to reach a concentration of 0.6 mol L^{-1}, thus leading to a citric acid:(Fe+La) molar ratio of 1. Further, 25 µL ethylene glycol (99.5 %, Fluka) and 700 µL aqueous ammonium hydroxide (25%, Fluka) were added to facilitate the polymerization and adjust the pH, respectively. The solution was then heated under reflux at 50 °C overnight. Subsequently, the precursor sol was further heated at 55 °C in air until the total volume of the sol was decreased to one half of its initial value.

Si(100) substrates (Sil'Tronix) were cleaned by successive immersion in acetone (10 minutes) and isopropanol (10 minutes) in an ultrasonic bath. After rinsing with millipore water, the substrates were immersed in freshly prepared piranha solution (vol. 1:1 H_2O_2/H_2SO_4) for 20 minutes and rinsed well with millipore water and stored in the same for transportation. Before deposition, the substrate was characterized confirming a 1-2 nm of amorphous silica layer covering Si(100).

The sol was then deposited at room temperature on the dried SiO_2/Si(100) substrates by spin coating with a typical speed of 2000 rpm. The layers were further heated up to 150 °C for 2 hours (ramp: 0.5 °C min^{-1}) and subsequently heated up to 650 °C for 4 hours (ramp: 1.0 °C min^{-1}) in a muffle oven. A thin film appearing transparent, slightly orange-coloured and showing only few, tiny cracks was thus obtained.

2.2 X-Rays Diffraction (XRD)

The X-ray diffraction structural characterization of the $LaFeO_{3\pm\delta}$ film was carried out using a 9 kW Rigaku Smartlab rotated anode X-ray diffractometer using Cu K_α (1.5418 Å) wavelength, operated in Bragg-Brentano reflexion geometry. To avoid any saturation of the detector due to the (004) peak of the oriented Si substrate, the sample was intentionally disoriented by 2°, once it was verified that the deposition was not epitaxial but polycrystalline.

2.3 Raman Analyses

Raman spectra were recorded using an Ar^+ (488 nm) laser for excitation, the power at the sample was adjusted using neutral density filters for the purpose of the experiments. The laser beam was focused at the surface of layered samples using a 100X microscope objective (NA 0.9). The Raman signal was collected in backscattering mode using the same objective through a confocal hole of 100 µm diameter. The scattered light was dispersed via a spectrometer equipped with a 1800 grooves grating (typical spectral resolution at 488 nm: 2 cm^{-1}) and finally analysed using a Peltier-cooled CCD (Horiba Labram HR).

2.4 Surface properties

Atomic Force Microscopy (AFM) analysis The surface morphology of the films was locally investigated using a commercial atomic force microscope (AFM) (MFP-3D, Asylum Research) working in AC

-or tapping- mode under ambient conditions. Si tips (Nanoworld Arrow-NC probes) with cantilever stiffness of 40 Nm^{-1} were used as local probes.

Time of Flight -Secondary Ion Mass Spectrometry (ToF-SIMS) analysis ToF-SIMS depth profiling was performed in positive mode using a TOF.SIMS5 instrument (ION-TOF, GmbH Germany), equipped with a bismuth liquid metal ion gun. Pulsed Bi^+ primary ions have been used for analysis (25 keV, 1 pA) while the sputtering was performed using a Cs^+ (1 keV, 80 nA) ion source running in non-interlaced mode [14]. The analysed surface was 100 µm X 100 µm centred over the 300 µm X 300 µm sputtered crater. Charging effects were compensated using pulsed low energy electrons (20 eV).

X-Ray Photoelectron Spectroscopy (XPS) analysis XPS characterization was carried out using the Kratos AXIS $Ultra^{DLD}$ spectrometer using a monochromatic Al K_α X-ray source (10 mA, 12 kV). C 1s, O 1s, Fe 2p and La 3d high resolution spectra were obtained using a 20 eV pass energy while keeping a pressure in the analysis chamber below 5×10^{-9} mbar during analysis. All spectra have been calibrated by giving the adventitious C 1s spectral component (C-C, C-H) a binding energy (BE) of 284.8 eV. A Shirley background [15] was subtracted from the spectra for quantification. The analysed area was about 300 µm X 700 µm.

Low-Energy Ion Scattering (LEIS) analysis LEIS experiments were run using a Qtac100 instrument (ION-TOF GmbH) under a working pressure range of 1×10^{-8} mbar. The samples were analysed using a 3 keV $^4He^+$ primary ion beam directed perpendicular to the target surface. The beam current was typically set to 5 nA. The experiments have been performed at various ionic doses, the analysed area was kept 1000 µm X 1000 µm. The samples were treated *in situ* under atomic oxygen plasma prior to LEIS analyses.

3 Results and Discussion

3.1 Surface morphology of LFO films

The 100X magnification picture of LFO, presented in Fig. 1a shows leaf-like patterns with orange ridges and dark blue gullies. The AFM image shown in Fig. 1b revealed that the ridges are consistent with zones featuring thicker deposits while gullies are characteristic of thiner $LaFeO_{3\pm\delta}$ layers. The peak-to-valley roughness reaches 160 nm while the average level of thickness is equal to 70 nm±10 nm.

Fig. 1c shows that the LFO film is made of nano-sized aggregates similar in size and shape to those observed in powders prepared from the citrate-route [16]. The root mean squared roughness (RMS), R_q, defined by $R_q = \sqrt{\frac{1}{n}\sum_{i=1}^{n} y_i^2}$, where y_i is the level of the i^{th} of n data points, was found to reach about 15.6 nm. Interestingly, the average radius of $LaFeO_{3\pm\delta}$ nanocrystallites from Figure 1c reaches 68 nm ± 3 nm, which matches well the depth of the deposit. This suggests that a single

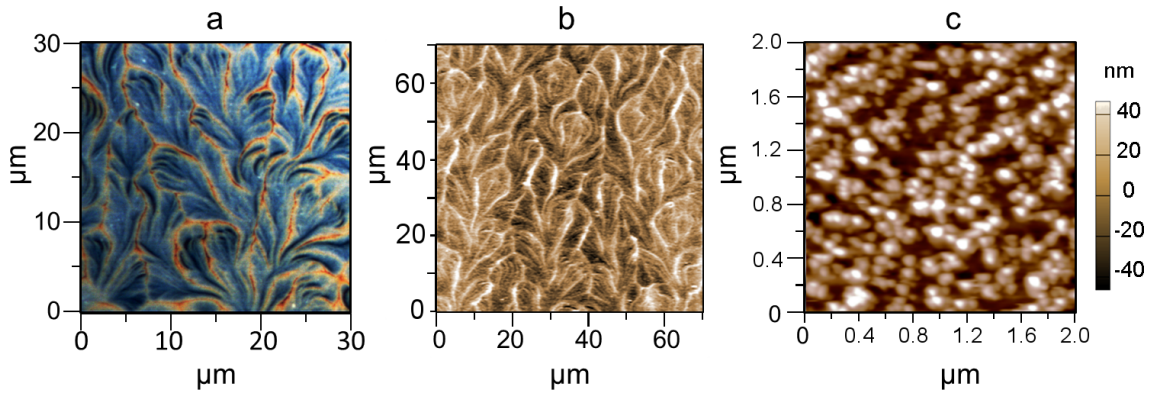

Figure 1: a: 100X magnification optical microscopy image, b: large-scale AFM image and c: AFM image on smaller area of LFO film.

layer of $LaFeO_{3\pm\delta}$ nanocrystals was deposited. It is to be noticed from Fig.1c, however, that between the$LaFeO_{3\pm\delta}$ nanocrystals nanosized voids are present.

3.2 Structure of LFO layers

3.2.1 X-Ray diffraction (XRD)

The diffraction pattern of the LFO layer displayed in Fig. 2 shows every reflection of the polycrystalline perovskite $LaFeO_{3\pm\delta}$ crystallised in orthorhombic lattice with lattice constants a=5.553 Å, b=5.563 Å and c=7.867 Å (space group: Pbnm) [17].

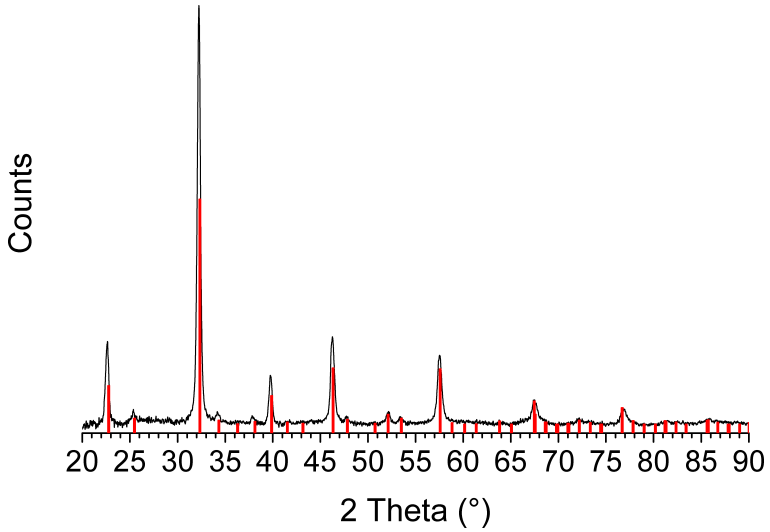

Figure 2: X-ray diffractogram of $LaFeO_{3\pm\delta}$ thin film; red stick diagram: diffraction pattern of $LaFeO_{3\pm\delta}$ (PDF 74-2203)

No reflection of any other crystalline phase such as La_2O_3, $La(OH)_3$ or Fe_2O_3 is observed.

3.2.2 Raman spectroscopy

The typically analysed sample depth is approximately 1 µm, which is one order of magnitude higher than the film's thickness. As a result, the Raman spectra recorded by focusing the laser beam at the surface of the layers are largely dominated by the signature of crystalline silicon found in bare SiO_2/Si(100), as can be seen in the spectra presented in Fig. 3, bottom.

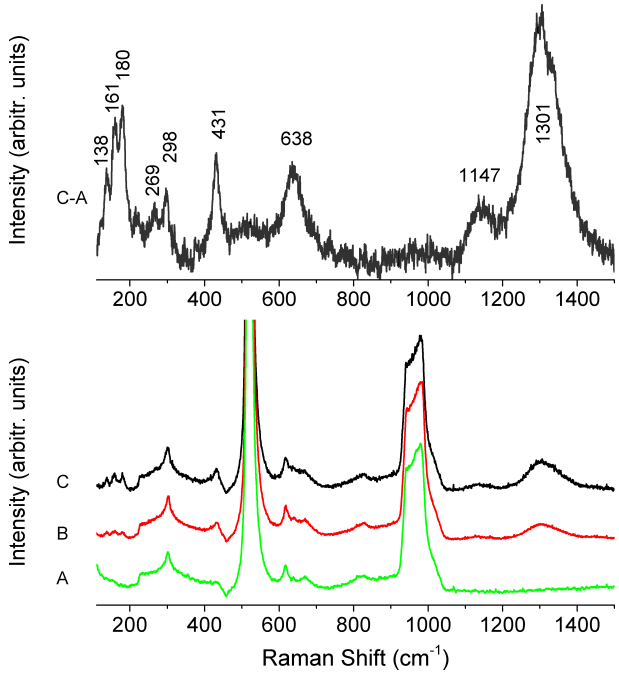

Figure 3: Bottom: Raman spectra of bare SiO_2/Si(100) (A) and of LFO thin film recorded in either a gully (B) or a ridge region (C). Top: Difference spectrum (C-A); $\lambda_{exc.}$=488 nm, acquisition time: 30 s, three scans were averaged.

However, the signature of polycrystalline lanthanum orthoferrite (LFO) can be handily retrieved by subtracting the Raman spectrum of the LFO thin film by the one of pure Si recorded under the same conditions. The difference spectrum, presented on top of Figure 3 C-A is similar in every respect to the Raman profile of the very same materials shaped as powders [9]. The assignment of the Raman bands of LFO have been already largely reported [18–20]. In brief, the modes below 200 cm^{-1} are related to La motions, the doublet of bands observed at 269 and 298 cm^{-1} are oxygen octahedral tilt (T) modes while the band at 431 cm^{-1} is assigned to the bending vibration of FeO_6 octahedra. The band at 638 cm^{-1} is assigned to Fe-O and La-O stretch vibrations. Broad bands of relatively high intensity are also detected at ~1147 and ~1300 cm^{-1}, which were previously assigned to second order scattering of IR-active longitudinal optic (LO) phonon modes. To sum up, in spite of the relatively low share of LFO phase as compared to the volume probed by Raman spectroscopy, LFO bands of high enough intensity are detected, which paves the way to further *operando* Raman analyses.

3.3 Surface analysis of LFO thin films

X-ray Photoelectron Spectroscopy (XPS) The XPS spectra of the $LaFeO_{3\pm\delta}$ thin film for C 1s, La 3d, Fe 2p, and O 1s are presented in Fig. 4. The C 1s photopeak presents an aliphatic peak together with weaker features at higher binding energies (BE) assigned to hydroxyl and carbonyl surface contaminations. The peak at BE of 289.2 eV with 11% of the total carbon peak area is attributed to the presence of adsorbed carbonate species at the surface of the $LaFeO_{3\pm\delta}$ film, as was previously also observed in the lanthanum-based corresponding powders [8].

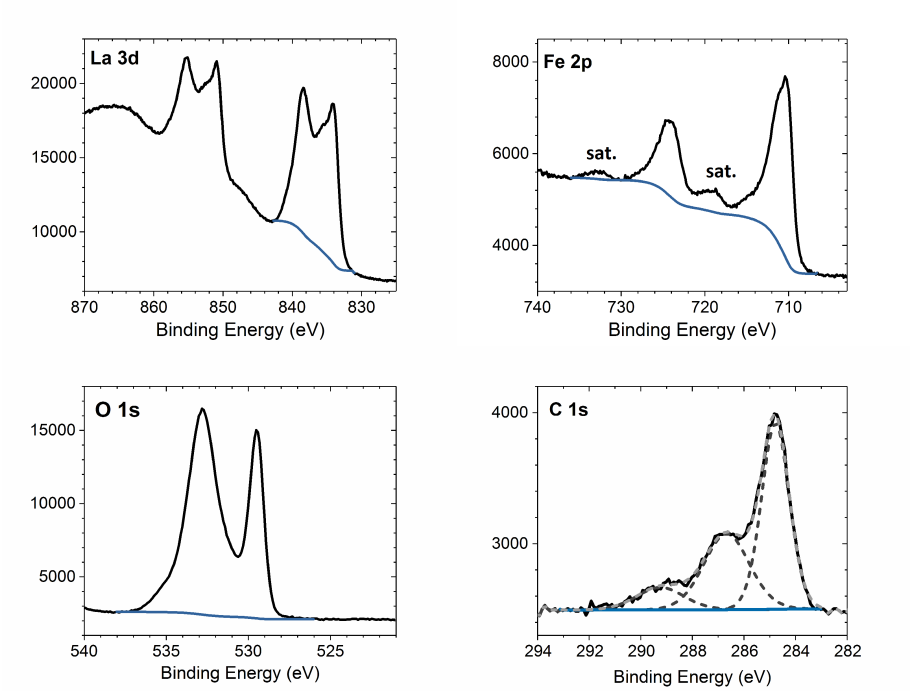

Figure 4: La 3d, Fe 2p, O 1s and C 1s spectra of $LaFeO_{3\pm\delta}$ thin film

The high-resolution spectrum of La 3d exhibits two peaks localized at 834.3 eV and 851.0 eV corresponding to the spin-orbit splitting of La $3d_{5/2}$ and La $3d_{3/2}$ of La^{3+} ion in its oxide form [21–24]. Each of the spin-orbit peak is further split by multiplet splitting components. The multiplet structure associated to La $3d_{5/2}$ peak shows a magnitude of 4 eV. This value corresponds to the presence of lanthanum hydroxide [21]. Indeed, owing to the reactive nature of La compounds which react in ambient air with water and CO_2 to form La hydroxides and carbonates, it is possible that this La 3d component is consisting of contributions from surface hydroxides and carbonates besides the mixed oxide. The binding energies of Fe $2p_{3/2}$ and Fe $2p_{1/2}$ are 710.5 eV and 724.2 eV, respectively, which is in line with the BE of Fe^{3+} ions in their oxide form. This is further confirmed by the 8.6 eV BE separation between the main Fe $2p_{3/2}$ peak and its satellite (sat.), characteristic of Fe^{3+} [25]. La 3d and Fe 2p core-level spectra thus revealed that both La and Fe stand in +3 oxidation state and their respective areas allows to calculate an atomic La:Fe ratio of 1.8. Only the La $3d_{5/2}$ peak was considered for quantification keeping in mind the overlapping of La MNN Auger peak with the La $3d_{3/2}$ component [21]. Compared to the

nominal composition, the $LaFeO_{3\pm\delta}$ thin film exhibits an excess of lanthanum at the surface whose value is close to what has been already reported on powdered samples [8].

The high-resolution spectrum of O 1s of the perovskite film is dominated by two intense components at 529.5 eV and 532.8 eV. The first one is in line with previous studies of contribution of bulk oxygen lattice involved in lanthanum oxide and iron oxide groups [21, 24, 26]. The second contribution centered at 532.8 eV is assigned to oxygen from hydroxyl groups (~ 531 eV), organic oxygen (~ 532 eV) and silica due to the existence of a silica over the Si substrateappearing from the voids arising from inhomogeneity of the film at both micro- and nanoscale, as discussed previously.

Low-Energy Ion Scattering (LEIS) The composition of the outermost surface of the $LaFeO_{3\pm\delta}$ thin film was investigated by means of LEIS and the corresponding spectra are presented in Fig. 5. Under static conditions, as in Fig. 5a, both La and Fe feature low-intensity scattering peaks detected at 2671 and 2313 eV, respectively, which confirms that the outermost $LaFeO_{3\pm\delta}$ surface contains both La and Fe species. The coverage of the $LaFeO_{3\pm\delta}$ nanocrystals over the silica/silicon surface induced inter-particle voids, see Fig. 1c, which can explain the detection of the low intensity Si peak at 1760 eV. Upon increasing the ionic dose (see, for example, Fig 5c, d and e), both Fe and La peaks were found to gradually and jointly increase in intensity.

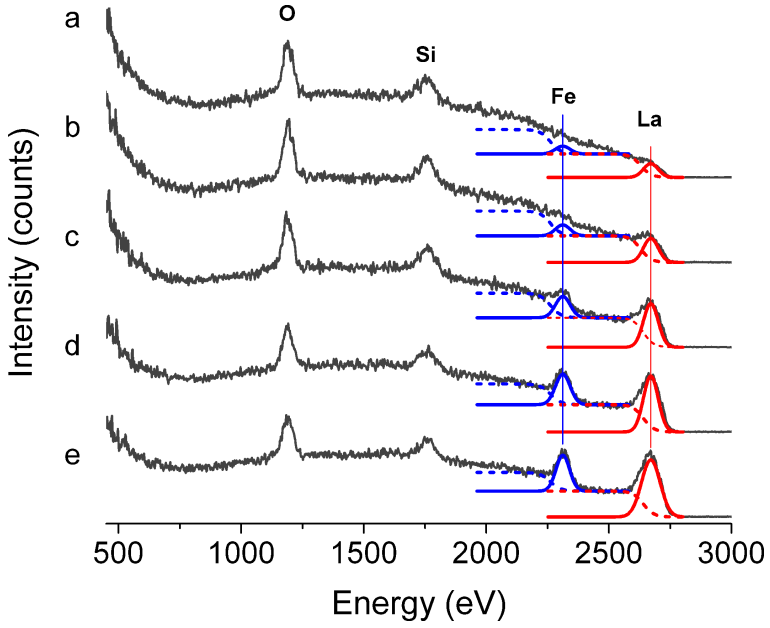

Figure 5: $^4He^+$ at 3 keV LEIS spectra of $LaFeO_{3\pm\delta}$ thin film recorded using an ionic dose of a: 2.0×10^{14} cm^{-2}, b:1.5×10^{16} cm^{-2}, c: 5.9×10^{16} cm^{-2}, d: 1.1×10^{17} cm^{-2} and e: 1.5×10^{17} cm^{-2}; Note that the spectra are shifted by a constant offset for clarity

An attempt for getting more information on the composition of the extreme surface of the film as probed by LEIS was made by considering the areas of Gauss LEIS surface peaks of Fe and La , further denoted as A_{Fe} and A_{La}, as a function of the ionic dose applied. The LEIS peaks areas presented in Fig. 6.

The extrapolated values of the raw areas of both La and Fe surface peaks at zero ionic dose suggest that both lanthanum and iron species are found in the extreme surface of the perovskite film. Besides, the $\frac{A_{La}}{A_{Fe}}$ ratio, plotted against the ionic dose in Fig. 6, approaches a constant value close to 2. This suggests that, within the sample depth investigated by LEIS, the lanthanum excess evidenced by XPS translates into a relatively stable La/Fe ratio.

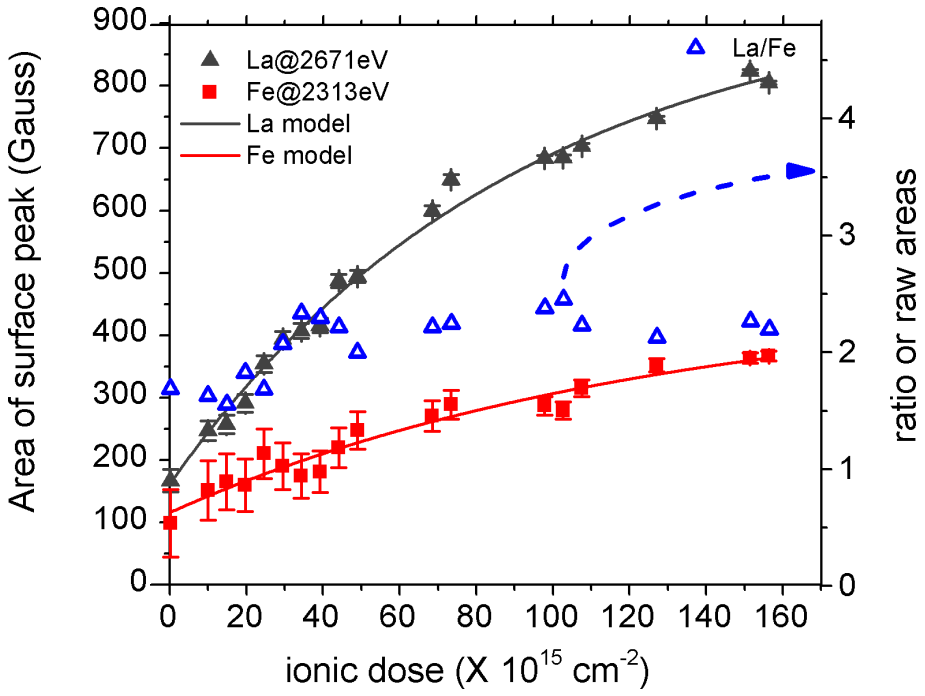

Figure 6: Evolution of the areas of Gauss profiles respectively assigned to Fe (red squares) and La (black triangles) surface peaks and the ratio of La:Fe raw areas (blue triangles) as a function of the applied ionic dose

3.3.1 Time of flight - Secondary Ions Mass Spectrometry (ToF-SIMS)

The elemental depth profile was built using the relative SIMS intensities of the Cs_2O^+ (281.80 a.m.u), $CsFe^+$ (188.84 a.m.u), $CsLaO^+$ (287.80 a.m.u) and Si^+ (27.98 a.m.u) fragments, which are representative for O, Fe, La and Si-containing moieties, respectively. A constant sputter rate of 0.08 nm s^{-1} was estimated on the basis of the AFM data, thus making it possible to convert sputter time into sample depth. Fig. 7 shows the evolution of the normalised intensities of the most relevant fragments, as detailed above.

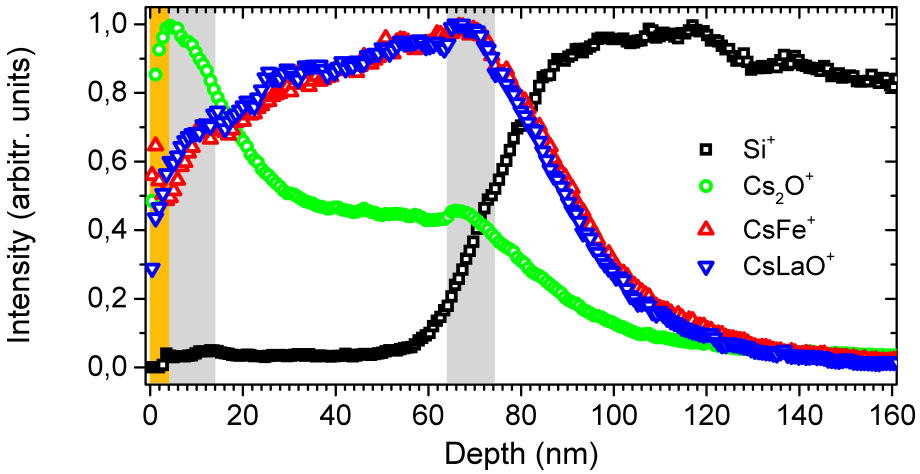

Figure 7: SIMS depth profile of Cs-enriched relevant fragments

A first layer of approximately 10 nm exhibits highest relative content in oxygen species, which can be related to contributions of carbonates species such as $La_2(CO_3)_3$ as well as hydroxyls from La, as suggested by our XPS results. Between 20 and 60 nm, both the concentrations of La- and Fe-containing moieties gently increase, as the contribution of oxygen declines. Having in mind that the $LaFeO_{3\pm\delta}$ phase is confirmed by XRD and Raman, we assume here that this moderate shift in the contribution of La, Fe and O-containing fragments does not reflect a genuine composition gradient, but is induced by an experimental bias. As a result, we propose that this region corresponds to a pure $LaFeO_{3\pm\delta}$ phase which does not exhibit significant carbonate content. Between 60 and 75 nm, the depth profile features the coexistence of La, Fe, Si and oxygen species, which corresponds to the $LaFeO_{3\pm\delta}/SiO_2/Si$ interface. Finally, only pure silicon is detected when the depth exceeds 120 nm. On the basis of the presented XPS and structural results, one would expect the depth profile to show a marked excess of La-containing fragments at the surface and a subsequent convergence of the normalised contributions of Fe- and La-containing species when entering the sample bulk. However, the depth profile shown here does not comply with this expectation at the outermost surface. Indeed, besides the skin effect and surface contaminants blurring the first five nanometers of SIMS intensities, both La- and Fe-moieties seems to evolve similarly.

An elemental mapping was also run over a wide sample surface and is presented in Fig. 8. It can be seen that La and Fe species are found in similar areas and that no obvious sizeable segregated domains

are detected within the investigated range.

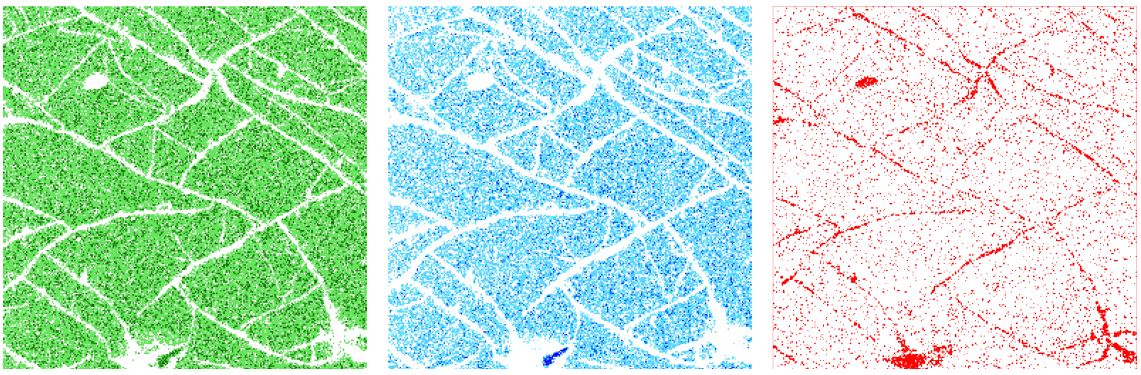

Figure 8: 500 µm X 500 µm maps of Fe^+ (left), LaO^+ (middle) and Si^+ (right) fragments distribution as afforded from ToF-SIMS experiments

4 Conclusion

A polycrystalline thin film of $LaFeO_{3\pm\delta}$ was prepared by spin coating over SiO_2/Si(100) using the polymerisable complex method. The $LaFeO_{3\pm\delta}$ layer was shown to retain the same structural and surface properties as the powdered solids, which makes the as-prepared thin film a relevant model catalyst for investigating bulk catalysts based on $LaFeO_{3\pm\delta}$. On the other hand, shaping $LaFeO_{3\pm\delta}$ into a thin film made it possible to attain unprecedented combined surface analyses. Moreover, the present work establishes the possibility to investigate such thin films using *in situ* Raman spectroscopy as well as advanced surface characterisation techniques in quasi-*in situ* or near-ambient pressure (NAP) XPS. This can enable us to establish relationships between the physico-chemical properties of perovskite model surfaces and the reactivity of the conventional catalysts.

Acknowledgements

The present work is part of the PARTIAL-PGMs project funded by the European Commission under the grant agreement # 686086. *Chevreul Institute (FR 2638), Ministère de l'Enseignement Supérieur et de la Recherche, Région Nord - Pas de Calais* and *Fonds Européen de Développement Régional (FEDER)* within the *Pôle Régional d'Analyses de Surface* and the *Contrat de Plan Etat-Région (CPER)* project "Chemistry and Materials for a Sustainable Growth" are acknowledged for supporting and fundings. T. Carlier is grateful to the *Région Nord-Pas de Calais* for its financial support to carry out this work.

References

[1] Pecchi G, Campos C, Peña O. Thermal stability against reduction of $LaMn_{1-y}Co_yO_3$ perovskites. Mater Res Bull. 2009;44(4):846–853.

[2] He H, Dai H, Au C. An investigation on the utilization of perovskite-type oxides $La_{1-x}Sr_xMO_3$ (M= $Co_{0.77}Bi_{0.20}Pd_{0.03}$) as three-way catalysts. Appl Catal B: Environ. 2001;33(1):65–80.

[3] Levasseur B, Kaliaguine S. Effects of iron and cerium in $La_{1-y}Ce_yCo_{1-x}Fe_xO_3$ perovskites as catalysts for VOC oxidation. Appl Catal B: Environ. 2009;88(3):305–314.

[4] Nishihata Y, Mizuki J, Akao T, Tanaka H, Uenishi M, Kimura M, et al. Self-regeneration of a Pd-perovskite catalyst for automotive emissions control. Nature. 2002;418(6894):164–167.

[5] Katz MB, Graham GW, Duan Y, Liu H, Adamo C, Schlom DG, et al. Self-regeneration of Pd–LaFeO3 catalysts: new insight from atomic-resolution electron microscopy. J Am Chem Soc. 2011;133(45):18090–18093.

[6] Kuc J, Zhang Y, Erni R, Yoon S, Karvonen L, Weidenkaff A, et al. Composition dependent self-regenerative property of perovskite-type oxides. Phys Status Solidi (RRL). 2015;9(5):282–287.

[7] Glisenti A, Pacella M, Guiotto M, Natile M, Canu P. Largely Cu-doped $LaCo_{1-x}Cu_xO_3$ perovskites for TWC: Toward new PGM-free catalysts. Appl Catal B: Environ. 2016;180:94–105.

[8] Schön A, Dujardin C, Dacquin JP, Granger P. Enhancing catalytic activity of perovskite-based catalysts in three-way catalysis by surface composition optimisation. Catal Today. 2015;258:543–548.

[9] Blanck D, Schön A, Mamede AS, Dujardin C, Dacquin JP, Granger P, et al. *In situ* Raman spectroscopic evidence of surface sites potentially involved in the enhanced activity of La-deficient materials in 3-way catalysis (TWC). Catal Today. in press;.

[10] Goodman DW. Model studies in catalysis using surface science probes. Chem Rev. 1995;95(3):523–536.

[11] Gunter PL, Niemantsverdriet J, Ribeiro FH, Somorjai GA. Surface science approach to modeling supported catalysts. Catal Rev. 1997;39(1-2):77–168.

[12] Klisinska A, Mamede AS, Gaigneaux EM. Spin-coating of mixed citrate complexes as a versatile route to prepare films of transition metal multi-element oxide model catalysts with controlled formulation and crystalline structure. Stud Surf Sci Catal. 2006;162:745–752.

[13] Liu X, Ji H, Gu Y, Xu M. Preparation and acetone sensitive characteristics of nano-$LaFeO_3$ semiconductor thin films by polymerization complex method. Mat Sci Eng B-Solid. 2006;133(1):98–101.

[14] Iltgen K, Bendel C, Benninghoven A, Niehuis E. Optimized time-of-flight secondary ion mass spectroscopy depth profiling with a dual beam technique. J Vac SciTechnol A. 1997;15(3):460–464.

[15] Shirley DA. High-Resolution X-Ray Photoemission Spectrum of the Valence Bands of Gold. Phys Rev B. 1972 Jun;5:4709–4714.

[16] Murade P, Sangawar V, Chaudhari G, Kapse V, Bajpeyee A. Acetone gas-sensing performance of Sr-doped nanostructured $LaFeO_3$ semiconductor prepared by citrate sol–gel route. Curr Appl Phys. 2011;11(3):451–456.

[17] Marezio M, Dernier P. The bond lengths in LaFeO 3. Mater Res Bull. 1971;6(1):23–29.

[18] Andreasson J, Holmlund J, Rauer R, Käll M, Börjesson L, Knee CS, et al. Electron-phonon interactions in perovskites contaning Fe and Cr studied by Raman scattering using oxygen-isoptope and cation substitution. Phys Rev B. 2008;78:235103.

[19] Popa M, Frantti J, Kakihana M. Lanthanum ferrite $LaFeO_{3+\delta}$ nanopowders obtained by the polymerizable complex method. Solid State Ionics. 2002;154-155:437–445.

[20] Dubroka A, Humlíček J, Abrashev MV, Popović Z, Sapina F, Cantarero A. Raman and infrared studies of $La_{1-y}Sr_yMn_{1-x}M_xO_3$ (M= Cr, Co, Cu, Zn, Sc or Ga): Oxygen disorder and local vibrational modes. Phys Rev B. 2006;73(22):224401.

[21] Sunding M, Hadidi K, Diplas S, Løvvik O, Norby T, Gunnæs A. XPS characterisation of in situ treated lanthanum oxide and hydroxide using tailored charge referencing and peak fitting procedures. Journal of Electron Spectroscopy and Related Phenomena. 2011;184(7):399–409.

[22] Phokha S, Pinitsoontorn S, Maensiri S, Rujirawat S. Structure, optical and magnetic properties of LaFeO3 nanoparticles prepared by polymerized complex method. J Sol-Gel Sci Technol. 2014;71(2):333–341.

[23] Su H, Jing L, Shi K, Yao C, Fu H. Synthesis of large surface area LaFeO3 nanoparticles by SBA-16 template method as high active visible photocatalysts. J Nanopart Res. 2010;12(3):967–974.

[24] Thirumalairajan S, Girija K, Mastelaro VR, Ponpandian N. Surface morphology-dependent room-temperature $LaFeO_3$ nanostructure thin films as selective NO_2 gas sensor prepared by radio frequency magnetron sputtering. ACS Appl Mater Interfaces. 2014;6(16):13917–13927.

[25] Biesinger MC, Payne BP, Grosvenor AP, Lau LWM, Gerson AR, Smart RSC. Resolving surface chemical states in XPS analysis of first row transition metals, oxides and hydroxides: Cr, Mn, Fe, Co and Ni. Applied Surface Science. 2011;257(7):2717 – 2730.

[26] Ramana C, Vemuri R, Kaichev V, Kochubey V, Saraev A, Atuchin V. X-ray photoelectron spectroscopy depth profiling of La_2O_3/Si thin films deposited by reactive magnetron sputtering. ACS Appl Mater Interfaces. 2011;3(11):4370–4373.